Optimal wave focusing

Farhad Bazargani and Roel Snieder
Center for Wave Phenomena, Colorado School of Mines, Golden, CO 80401, USA

ABSTRACT
Focusing waves inside a medium has applications in various science and engineering fields, e.g., in medical imaging, ultrasound therapy, noninvasive surgery, nondestructive evaluation, and geophysics in areas such as imaging and focusing microseismic events. The goal in focusing is to concentrate the wave energy at a specific time and location inside a medium. Various techniques have been devised and used to achieve this goal. Time-reversal (TR) is a well-researched method that has been used routinely to focus acoustic and seismic waves. Here, we propose a new technique wherein wave focusing is cast as an optimization problem. The objective is to study the possibility of improving upon the performance of the existing focusing methods.

Key words: wave focusing, optimization, time-reversal, imaging, microseismic

1 INTRODUCTION

The objective in wave focusing is to determine the waveforms that, when transmitted through a medium, create a wavefield that concentrates at a specific time and location. Wave focusing is conceptually related to the problem of imaging, and hence finds important applications in areas such as exploration geophysics.

Several methods for focusing have been devised, including those based on inverse scattering (Haddadin and Ebbini, 1998; Broggini et al., 2012; Behura et al., 2012), phase conjugation (Parvulescu, 1961), and time-reversal (Fink, 1997). Time-reversal (TR) is a well-established focusing technique that is robust and effective in heterogeneous media. The method relies on the time-reversal invariance of the wave operator and spatial reciprocity (Fink et al., 2002; Snieder, 2004).

A time-reversal mirror (TRM) is an array of transducers, each capable of detecting and recording, time-reversing (last-in first-out), and retransmitting signals into the medium. The TR process consists of two basic steps (Figure 1). In the first, the wavefield generated at a source in the medium is recorded using a closed TRM surrounding the source. In the second step, the recorded waveforms are time-reversed, retransmitted through the medium, and propagated back to refocus approximately at the original source location. In a dissipative medium, time-reversal invariance is not satisfied. Spatial reciprocity alone, nevertheless, explains the robustness and efficiency of the TR process in many applications involving dissipative media (Fink, 2006).

TR focusing methods have now been implemented in a variety of physical scenarios. TR can be done in both physical and numerical (back-propagation) experiments. In both, one deals with propagation of a time-reversed field, but the propagation is real in a physical problem and simulated in a back-propagation numerical problem (Fink, 2006). Applications involving physical TR problems include medical imaging (Robert and Fink, 2008), lithotripsy, underwater acoustics, and nondestructive testing (Fink, 1997; Larmat et al., 2010).

TR back-propagation methods are applied in key areas of geophysics on both global and exploration scales. In global seismology, TR techniques are used for studying earthquake source mechanism and evolution, event location, explosion monitoring, and environmental applications of geophysics (Lu, 2002; Larmat et al., 2006, 2010). In exploration seismology, TR focusing is used in microseismic event location (Lu and Willis, 2008; McMechan, 1982; Xuan and Sava, 2010), fracking and reservoir monitoring (Shapiro, 2008), salt-flank imaging and redatuming seismic data (Lu, 2002), and migration (Berkhout, 1997). Reversed time migration, one of the most successful imaging techniques in exploration seismology, consists of three basic steps; time-reversal of the recorded data, propagation of source and receiver wavefields, and implementation of an imaging condition (McMechan, 1983; Schuster, 2002).

Despite these broad applications, the TR process has important theoretical limitations. In theory, for a broadband pulse emitted by an ideal point source, the returning field refocuses on a spot with dimensions on

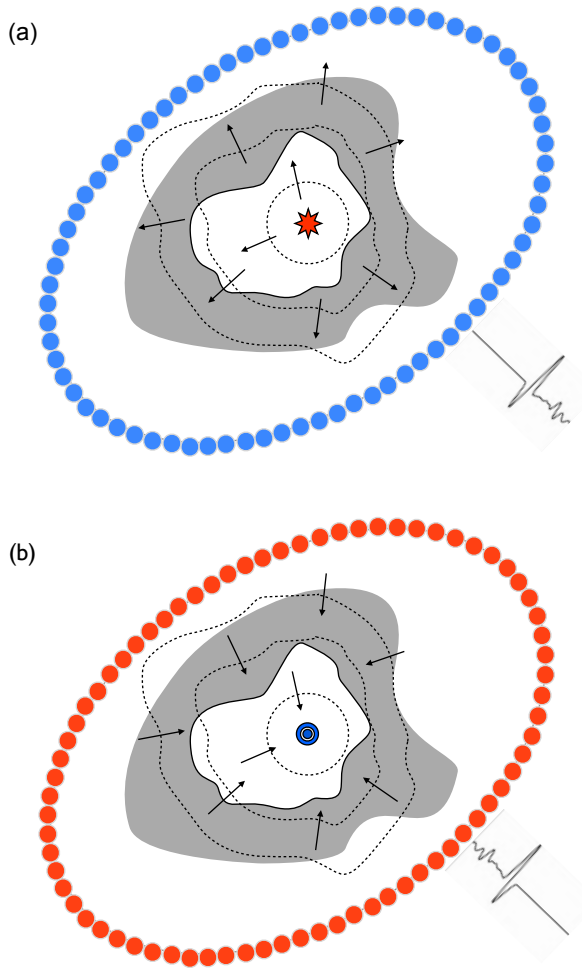

Figure 1. Illustration of a time-reversal experiment. (a) Forward propagation step: waves excited by a source travel through the complex medium and are recorded at stations marked as circles. (b) Back-propagation step: the recorded signals are reversed in time and re-emitted into the medium at the corresponding stations. The waves then propagate through the medium and converge on the original source location. Figure from (Lu, 2002).

the order of the smallest wavelength (Abbe diffraction limit). This is because evanescent waves containing source details smaller than the involved wavelengths cannot be sensed in the far-field. Therefore, this information is lost and causes the resolution of the process to be bounded by the diffraction limit (Fink, 1997).

TR focusing also has several practical limitations. From the experimental point of view, it is not possible to record and retransmit the wavefield everywhere on a surface that fully encloses the source. In practice, the wavefield is sampled at spatially sparse locations. Also, it is often not practical to surround the area of interest with a full-aperture TRM, so a finite-aperture TRM is used instead. This imperfect acquisition causes an increase in the dimension of the point-spread function (Fink, 2006). Another problem is that in real applications of TR-focusing, the media are dissipative and time-reversal invariance of the wave equation does not hold valid in dissipative media. As shown by Fink (2006), however, even in a dissipative medium, the TR process always maximizes the output amplitude received at the source at the focal time although it does not impose any constraints on the field around the focus. For example, side lobes can be observed around the source.

Several studies have been devoted to investigate these limitations and alleviate their effect to improve the TR procedure. Tanter et al. (2000, 2001), Aubry et al. (2001), and Montaldo et al. (2003) present the spatio-temporal inverse-filter method, a new focusing technique based on the inverse of the wave propagator between a source and elements in a TRM. For a lossless medium, the inverse filter method yields the same result as that of the TR method, but in the presence of attenuation, the spatio-temporal inverse filter methods are more effective than is the TR method.

Research on the connection between medium complexity and the size of the focal spot has shown a direct relationship between complexity of medium and resolution in TR focusing; the more complicated the medium between the source and the TRM, the sharper the focus (Blomgren et al., 2002; Fink, 2008; Vellekoop et al., 2010). This is because a finite-aperture TRM acts as an antenna that uses complex environments to appear wider than it actually is, resulting in a focusing capability that is less dependent on the TRM aperture. In media made of random distribution of sub-wavelength scatterers, a time-reversed wave field can interact with the random medium to regenerate not only the propagating but also evanescent waves required to refocus below the diffraction limit (super-resolution). Schuster et al. (2012) demonstrate a method that uses evanescent waves generated by scatterers in the near-field region of seismic sources to achieve super-resolution.

In this paper, we propose an alternative approach to wave focusing wherein the problem is cast as an optimization problem. As discussed above, the mainstream focusing methods currently in use are not optimal for real problems because of imperfect acquisition, attenuation, and the diffraction limit. The motivation for this research is to improve upon the existing techniques especially where such techniques do not perform optimally in dealing with the inherent and unavoidable limitations encountered in real focusing problems. In section 2, we lay out the theoretical foundation of the new focusing method and then,in section 3, compare our approach with other common focusing techniques. Section 4 is devoted to a numerical wave focusing experiment that demonstrates the implementation of the proposed method. We also provide a comparison of the

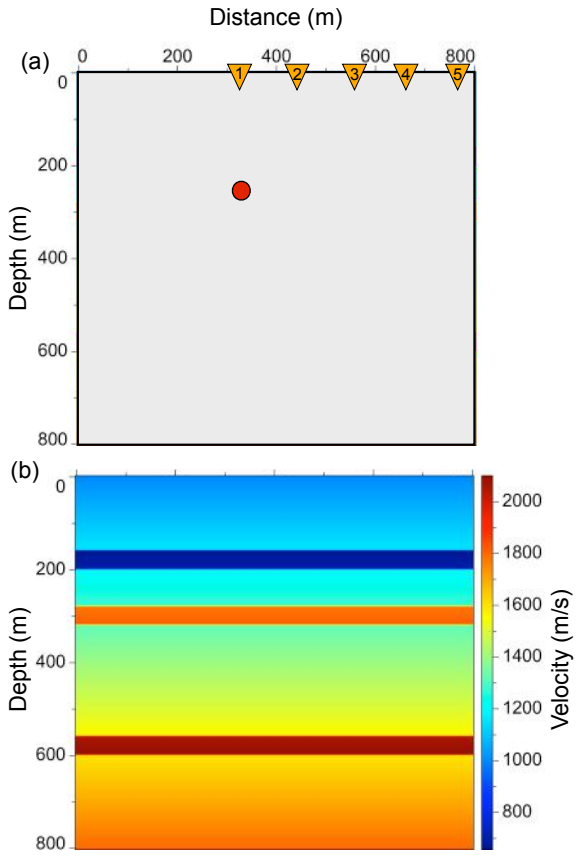

Figure 2. Configuration of the synthetic experiment (a) showing the locations of the sources (yellow triangles) and focusing target (red circle), and the assumed acoustic velocity model (b) for the medium.

focus achieved by the proposed method with the outcome of other focusing methods. Finally, in section 5, we discuss applications of the method in areas such as seismic imaging and microseismic event location, and elaborate on issues associated with each particular application.

2 FOCUSING AS AN OPTIMIZATION PROBLEM

Consider N sources at distinct locations $\mathbf{r}_i$ wherein each source is capable of transmitting predefined signals. The objective is to design signals such that, upon transmission, focuses optimally at a specific time and location inside the medium. Each source must work in concert with the others by injecting a signal that is tailored in amplitude and shape according to the specific medium, source geometry, and focusing target in order to achieve the best spatio-temporal focus.

If we denote the signal injected by the source at $\mathbf{r}_i$ as $a_i(t)$, then the superposed wavefield recorded at an arbitrary location $\mathbf{r}$ inside the medium is

$$u(\mathbf{r},t) = \sum_{i=1}^{N} a_i(t) * g(\mathbf{r},\mathbf{r}_i,t), \tag{1}$$

where $*$ is the convolution operator, and $g(\mathbf{r},\mathbf{r}_i,t)$ is the impulse response (Green's function) recorded at location $\mathbf{r}$ and corresponding to an impulsive source at location $\mathbf{r}_i$. Note that if the velocity of the medium is known, these Green's functions can be computed.

Convolution in the time domain corresponds to multiplication in the frequency domain. Therefore, considering the problem in the frequency domain, each frequency component of the wavefield u in equation 1 can be restated as a weighted sum of the corresponding frequency component $G(\mathbf{r},\mathbf{r}_i,\omega)$ of the Green's functions

$$u(\mathbf{r},\omega) = \sum_{i=1}^{N} a_i(\omega)\, G(\mathbf{r},\mathbf{r}_i,\omega), \tag{2}$$

where the weights $a_i(\omega)$ are the Fourier components of the injected signals.

The problem can now be restated as how to optimally determine the weights $a_i(\omega)$ in equation 2 so that the superposed field u in the time domain focuses at a desired location of focus $\mathbf{r}_f$ and at a desired time of focus (usually taken to be $t_f = 0$). Put another way, the goal is to have $u(\mathbf{r},t)$ as close as possible to $\delta(\mathbf{r}-\mathbf{r}_f)\delta(t)$, where δ denotes the Dirac delta function. In the frequency domain, this amounts to making each $u(\mathbf{r},\omega)$ as close as possible to $\delta(\mathbf{r}-\mathbf{r}_f)$. This goal can be achieved, for example, by minimizing an objective function defined as

$$J = \int |u(\mathbf{r},\omega) - \delta(\mathbf{r}-\mathbf{r}_f)|^2 d\mathbf{r}. \tag{3}$$

This condition is known as the *deltaness criterion* in the context of the method of Backus and Gilbert (BG) in inverse theory (Backus and Gilbert, 1968). A good description of this method is provided by Aki and Richards (1980) and Aster et al. (2012). Inserting equation 2 in objective function 3 and minimizing with respect to each $a_i(\omega)$ gives a linear system of equations of the form

$$\Gamma\mathbf{a} = \mathbf{g}^*, \tag{4}$$

where Γ is the $N \times N$ Gram matrix (Parker, 1994) with elements defined as

$$\Gamma_{ij} = \int G(\mathbf{r},\mathbf{r}_i,\omega)\, G^*(\mathbf{r},\mathbf{r}_j,\omega)\, d\mathbf{r}, \qquad i,j = 1,2,...,N, \tag{5}$$

$\mathbf{g}$ is an $N \times 1$ vector with components

$$\mathbf{g}_i = G(\mathbf{r}_f,\mathbf{r}_i,\omega), \qquad i = 1,2,...,N, \tag{6}$$

and the symbol $*$ denotes complex conjugate.

The linear system in 4 can be solved for the $N \times 1$ vector $\mathbf{a}$ for each frequency. These $\mathbf{a}_i(\omega)$ vectors consti-

tute the Fourier coefficients for the signals that must be transmitted by each source at $\mathbf{r}_i$ to achieve an optimal focus at $\mathbf{r}_f$.

3 COMPARISON WITH OTHER TECHNIQUES

The Backus and Gilbert (BG) focusing method, introduced in section 2, is closely related to other techniques commonly in use. As explained below, particular choices of the Gram matrix Γ in equation 4 can reduce the BG method to other methods such as time-reversal or the deconvolution method presented by Ulrich et al. (2012).

First, we discuss the connection between the BG method and the TR method: Replacing Γ in equation 4 by the identity matrix I gives

$$\mathbf{a} = \mathbf{g}^*. \tag{7}$$

As before, this equation gives each frequency component of the vector $\mathbf{a}$. Now, since complex conjugation in the frequency domain is equivalent to time-reversal in the time domain, the new system of equations 7 describes exactly the same process as time-reversal in the time domain. Replacing Γ by the identity matrix amounts to cancelling the cross-talk between sources and having each source work independently to inject time-reversed Green's functions.

Next, we discuss the connection between the BG method and the deconvolution method: Setting the off-diagonal elements of Γ in equation 4 equal to zero ($\Gamma_{i,j} = 0$ for $i \neq j$), and solving the system of equations for $\mathbf{a}$, gives

$$a_i(\omega) = \frac{G^*(\mathbf{r}_f, \mathbf{r}_i, \omega)}{\int G(\mathbf{r}, \mathbf{r}_i, \omega)\, G^*(\mathbf{r}, \mathbf{r}_i, \omega)\, d\mathbf{r}}, \quad i = 1, 2, ..., N. \tag{8}$$

In the deconvolution method (Ulrich et al., 2012), the same frequency components of the signals to be back-propagated for focusing are computed as

$$a_i(\omega) = \frac{G^*(\mathbf{r}_f, \mathbf{r}_i, \omega)}{G(\mathbf{r}_f, \mathbf{r}_i, \omega)\, G^*(\mathbf{r}_f, \mathbf{r}_i, \omega) + \epsilon}, \quad i = 1, 2, ..., N, \tag{9}$$

where ϵ is a regularization term, on the order of $|G(\mathbf{r}_f, \mathbf{r}_i, \omega)|^2$, added for stability of the solution. Notice the similarity between equations 8 and 9; both equations have the same numerator on the right hand side, the denominators are similar except for the integration over the spatial element in equation 8 and the regularization term ϵ in equation 9.

Based on the discussions above, we can say that, compared to the TR and deconvolution techniques, the BG method provides a more general solution to the wave-focusing problem. In other words, TR and deconvolution methods are special cases of the more-general BG method with particular choices of Γ. The elements

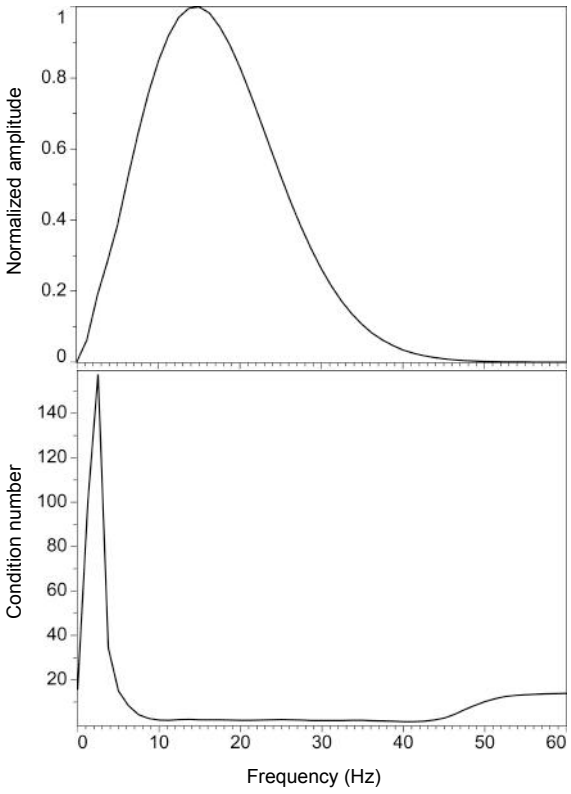

Figure 3. Amplitude spectrum (a) of the Ricker wavelet used as the source in the numerical experiment, and condition number (b) of the Gram matrix Γ as a function of frequency.

of the Gram matrix Γ hold crucial information about the configuration of the wave-focusing experiment, i.e., the relative positions of the sources with respect to the propagation medium and the focusing target. Each element plays a role in determining how the sources must work in tandem to inject the signals that achieve the optimum focusing at the target. The off-diagonal elements in Γ adjust the signal emitted by each source with respect to other sources.

4 SYNTHETIC DATA EXPERIMENT

To test the ideas presented above, we perform a numerical focusing experiment where we apply the BG method to focus wavefields at a target and compare the result with the focus achieve by other techniques such as TR, deconvolution, and TR with spectral whitening. TR with spectral whitening is a simple method for boosting the weak frequencies of a signal by dividing the components of the frequency band by their magnitudes ($a(\omega) \rightarrow a(\omega)/|a(\omega)|$) such that the resulting spectrum is flattened (whitened).

The configuration of the numerical experiment is

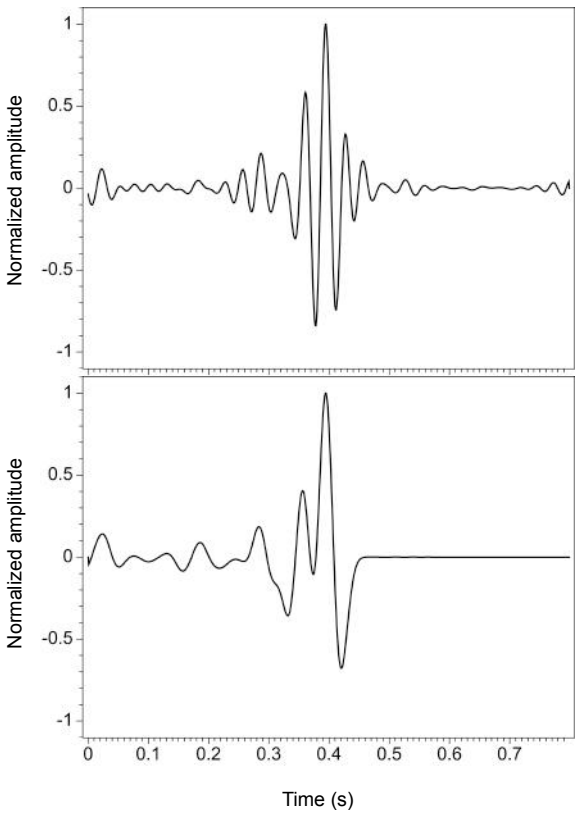

Figure 4. Signals required to be injected by source 2 shown in Figure 2 computed by (a) the proposed focusing method, and (b) time-reversal method.

shown in Figure 2a. The triangles represent the injection points (sources), the locations where the signals are emitted and numerically propagated to focus at the target, denoted by the red circle. The velocity model used for wave propagation is a 2D model (Figure 2b) consisting of a linearly varying background and three layers of low- and high-velocity contrasts inserted in the background. Wave propagation is simulated using an explicit finite-difference approximation of the 2D acoustic isotropic wave equation with absorbing boundary condition.

To form the Gram matrix Γ according to equation 4, we require an approximation of the impulse response of the medium $g(\mathbf{r}, \mathbf{r}_i, t)$. To compute the impulse response, at each injection point we inject a bandlimited Ricker wavelet with peak frequency of 16 Hz (Figure 3a) and forward propagate the wavefield in time. These wavefields are then transformed to the frequency domain and used in equation 5 to compute the elements of the 5×5 matrix Γ for each frequency. At this point, the right-hand side of equation 4 is also known because $\mathbf{g}_i = G(\mathbf{r}_f, \mathbf{r}_i, \omega) = G(\mathbf{r}, \mathbf{r}_i, \omega)|_{\mathbf{r}=\mathbf{r}_f}$.

Solving equation 4 for each frequency gives the Fourier coefficients $\mathbf{a}(\omega)$ of the signals that, upon injection, create wavefields that optimally focus at the target. Figure 4a shows one such signal computed for injection point 2. The signal, of the same injection point computed using the TR method, is shown in Figure 4b for comparison. Note the higher frequency content of the optimally computed signal (Figure 4a) compared to the time reversed signal (Figure 4b). Also, note the presence of noncausal energy between 0.45 s and 0.8 s (energy at times prior to the first arrival in the original recorded signal) in the optimally computed signal in Figure 4a.

To compare the effectiveness of the different wave-focusing methods, Figures 5a, b, c, and d show snapshots of the wavefield associated with the BG, TR, deconvolution, and TR with spectral whitening, respectively. As is evident in these snapshots, the BG method has outperformed the other methods in achieving a more concentrated spatial focus in this synthetic experiment.

5 DISCUSSION

5.1 Alternative deltaness criteria

The deltaness criterion defined as minimizing objective function 3 is not the only and probably not the best option. Other formulations of the deltaness criterion have been suggested and used in the inverse theory literature (Backus and Gilbert, 1968; Aki and Richards, 1980; Parker, 1994; Aster et al., 2012).

The focused fields shown in Figure 5 illustrate a possible motivation for trying other deltaness criteria. Even though our method shows a better spatial focus in Figure 5a compared to TR in Figure 5b, energy is present around the focus in the side lobes.

To reduce this side energy, we can use an objective function in which energy at distances farther away from the focusing target is penalized. One such objective function suggested by (Backus and Gilbert, 1968) is

$$W = \int (\mathbf{r} - \mathbf{r}_f)^2 \left| u(\mathbf{r}, \omega) \right|^2 d\mathbf{r}, \tag{10}$$

subject to the constraint

$$\int \left| u(\mathbf{r}, \omega) \right| d\mathbf{r} = 1, \tag{11}$$

where the weight factor $(\mathbf{r} - \mathbf{r}_f)^2$ in the integrand of expression 10 is responsible for penalizing the side energy. Note that depending on the specific requirements of a wave focusing problem, other weight factors can also be used. Minimizing the energy in the side lobes could be essential for some applications of wave focusing, e.g., in imaging. In other applications such as microseismic event location it might not be as important.

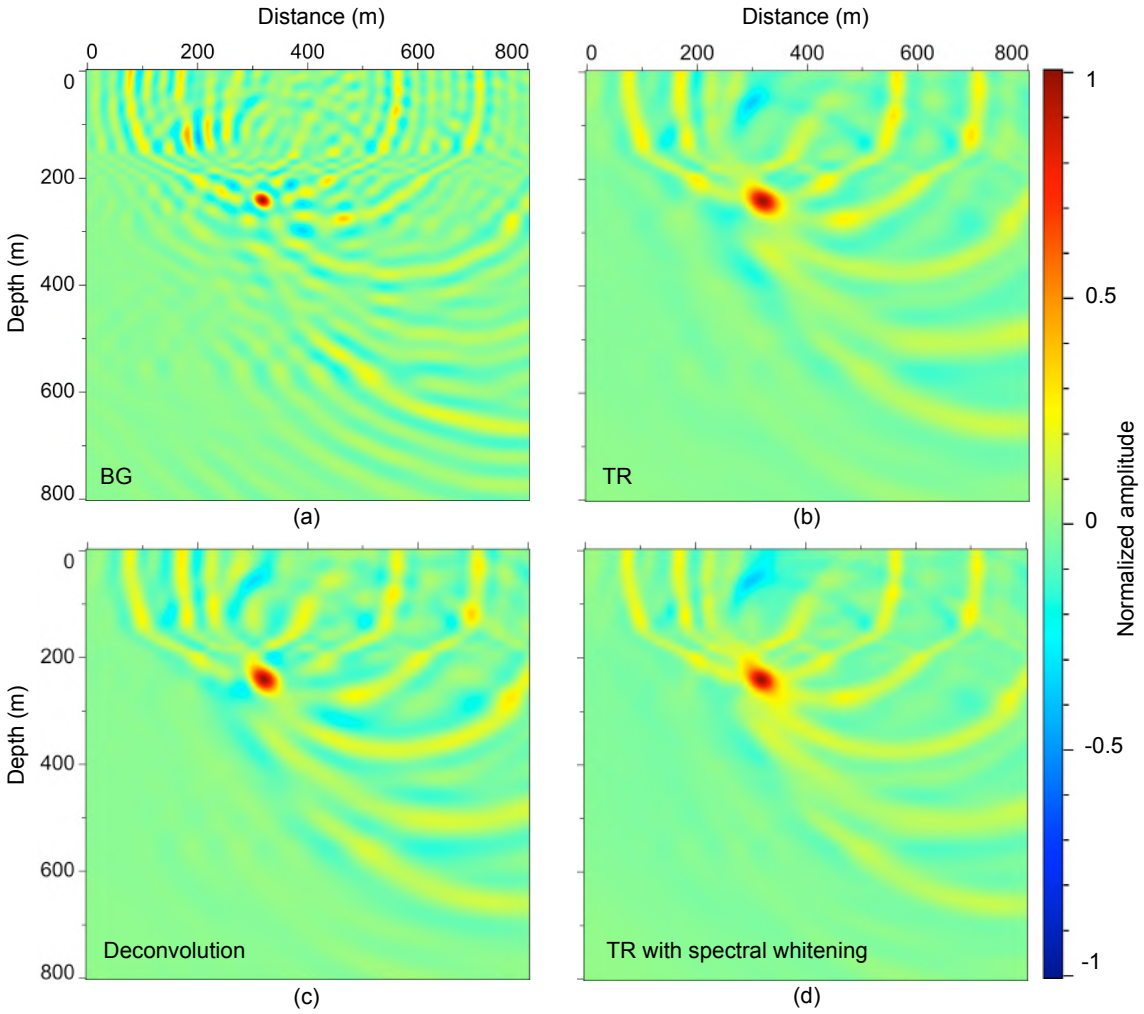

Figure 5. Results of the numerical focusing experiment of section 4 using noise-free data. The plots show the snapshots of propagating wavefields at the time of focus for (a) BG (the proposed method), (b) time-reversal, (c) deconvolution , and (d) time-reversal with spectral whitening.

5.2 Application in imaging

The Backus and Gilbert method presented in this paper to enhance focusing can also be used to enhance reverse-time-migration (RTM) imaging. Here, we show how the two ideas are connected and propose a method to combine them.

In the space-time domain, RTM is formulated as

$$\mathbf{m}_{mig}(\mathbf{r}) = \int [g(\mathbf{r}_g, \mathbf{r}, -t) * d(\mathbf{r}_g, \mathbf{r}_s, t)] \otimes_{t=0} [w(t) * g(\mathbf{r}, \mathbf{r}_s, t)]\, dg, \qquad (12)$$

where subscripts s and g stand for source and receiver, respectively, $\otimes|_{t=0}$ denotes the zero-lag cross-correlation, $\mathbf{m}_{mig}(\mathbf{r})$ represents the reflectivity distribution perturbed from the background medium, $g(\mathbf{r}, \mathbf{r}_s, t)$ denotes the Greens function for a specified background medium with a source at $\mathbf{r}_s$ and a receiver at $\mathbf{r}$, and $d(\mathbf{r}_g, \mathbf{r}_s, t)$ is the reflected wave recorded by the geophone at $\mathbf{r}_g$ due to a source with wavelet $w(t)$ shot at $\mathbf{r}_s$. The integration is over the data-space geophone variable denoted by $\mathbf{r}_g$.

By rearranging equation 12, Schuster (2002) introduces generalized diffraction-stack migration as an alternative implementation and interpretation of RTM. In generalized diffraction-stack migration, the migration image $\mathbf{m}_{mig}(\mathbf{r})$ can be interpreted as the zero-lag cross-correlation of the shot gather data $d(\mathbf{r}_g, \mathbf{r}_s, t)$ with a focusing kernel defined as

$$f(\mathbf{r}_s, \mathbf{r}, \mathbf{r}_g, t) = g(\mathbf{r}_g, \mathbf{r}, t) * w(t) * g(\mathbf{r}, \mathbf{r}_s, t). \qquad (13)$$

We show in Appendix A that, using a method similar to that described in section 2, we can optimize the focusing kernel 13 for each shot and for specific targets

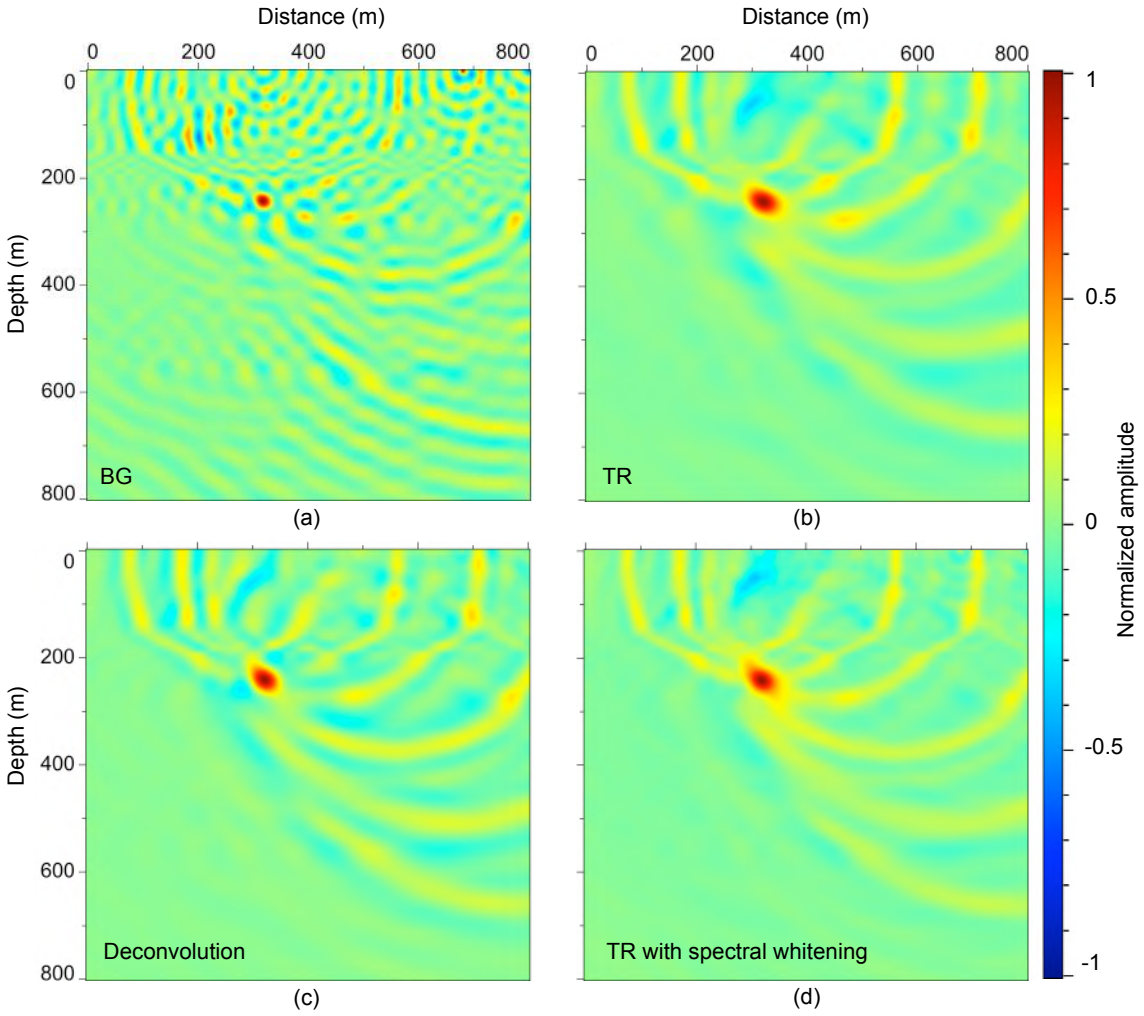

Figure 6. Same results as in Figure 5 for the same data plus bandlimited noise to simulate a microseismic location experiment. The plots show the snapshots of propagating wavefields at the time of focus for (a) BG (the proposed method), (b) time-reversal, (c) deconvolution, and (d) time-reversal with spectral whitening.

in the image. Using an optimized focusing kernel in implementation of the generalized diffraction-stack migration could enhance the resolution of the migration image and reduce the acquisition foot print in the image.

Least-Squares Migration (Nemeth et al., 1999) is an effective imaging method that deals with imaging problems resulting from imperfect acquisition. In this respect, one interesting question to address is how the proposed optimized generalized-diffraction stack migration scheme compares with the least-squares migration.

5.3 Application in microseismic event location

Locating seismic sources is an important problem in earthquake seismology and microseismic monitoring (Rentsch et al., 2007). Techniques based on time-reversal focusing are commonly used in seismology for event location (Larmat et al., 2010). Therefore, the effectiveness of such techniques is bounded by the same issues that limit the efficacy of TR focusing, i.e., diffraction limit, attenuation, and imperfect acquisition.

For this reason, the BG methodology proposed to enhance TR focusing can be particularly useful in source-location applications. For example, note that $g(\mathbf{r}_f, \mathbf{r}_i, \omega)$ in equation 6 is the impulse response of a source at $\mathbf{r}_i$ recorded at $\mathbf{r}_f$, and reciprocity implies that $g(\mathbf{r}_f, \mathbf{r}_i, \omega) = g(\mathbf{r}_i, \mathbf{r}_f, \omega)$. In the context of seismic event location, the Green's function $g(\mathbf{r}_i, \mathbf{r}_f, t)$ represents the microseismic or earthquake data recorded in the field at each receiver location.

The presence of noise in field data is an important matter that needs careful attention in applying BG focusing to event location. With noisy data, equation 4

must be modified as

$$\Gamma \mathbf{a} = \mathbf{g}^* + \boldsymbol{\eta}, \tag{14}$$

where $\boldsymbol{\eta}$ denotes the noise vector. In this case, Γ must be computed according to equation 5 using a velocity model, which is ideally accurate, and $\mathbf{g}$ represents the data measured in the field, so it does not need the velocity model. Even when the velocity model is not accurate, using the Γ matrix computed based on this inaccurate velocity is better than ignoring it altogether as is done the case in time-reversal. The stability of the solution $\mathbf{a}$ in equation 14 depends on the condition number of the Gram matrix Γ, which itself depends on the configuration of the receivers (injection points) and the medium.

Figure 3b shows the condition number of Γ as functions of frequency for the synthetic example of section 4. For the particular configuration and velocity model of this experiment, Γ is well-conditioned for most frequencies in the signal bandwidth (see Figure 3b). Only at the low and high ends of the signal bandwidth, where the amplitude of the frequencies approach zero, does the condition number of Γ increase. Therefore, here, the system of equations 14 is relatively stable and robust in the presence noise (for this particular experiment). In general, however, a combination of some sort of regularization and alternative deltaness criteria (section 5.1) might be used to stabilize equation 14.

We repeat the synthetic experiments of section 4 for data contaminated with bandlimited white noise with an rms signal-to-noise ratio of 5. The added noise in these experiments has the same bandwidth as the data. For real experiments, such as microseismic monitoring, a signal-to-noise ratio of 5 is rather high, but note that, in such experiments, the number of receivers is usually significantly larger than the number used in our synthetic example and this increase in the number of receivers improves the overall signal-to-noise ratio. Figures 6a, b, c, and d show snapshots of the focused wavefields produced by BG, TR, deconvolution, and TR with spectral whitening, respectively.

Comparison of the focused wavefields created by different focusing methods using noise-free and noisy data in Figures 5 and 6 reveals that the BG method can focus just as well in the presence of noise. Although, other methods are less sensitive to noise. Note the increase of side lobe energy in the result of BG focusing in Figure 6a compared to Figure 5a. The other three methods have produced almost the same focusing results for data with and without noise.

Another important consideration related to applying the BG focusing method to microseismic event location is the source mechanism. In the numerical examples shown in this paper, we have assumed a point source with an isotropic radiation pattern. The source mechanism for a microseismic event is, however, a double couple with its characteristic radiation pattern for both P and S waves. Therefore, it is more appropriate to use a deltaness criterion that takes assumed features of the source mechanism for microseismic events into account. The BG focusing technique can also be used for determining the optimal way to process and combine all different components of recorded microseismic data in order to achieve more accurate results in microseismic monitoring.

6 CONCLUSION

The ability of time-reversal (TR) methods to focus wave fields inside heterogeneous media is bounded by limitations caused by imperfect acquisition, attenuation, and the diffraction limit. To go beyond these limitations, we present a solution by formulating wave focusing as an optimization problem. Solving this optimization problem gives the needed signals for transmission to the medium to get the best focus. These signals are optimized for the configuration of the injection points, velocity of the medium, and the focusing target.

Our numerical tests show that the Backus and Gilbert (BG) approach is capable of achieving a significantly more compact focus compared to that of other common focusing techniques (e.g., TR, deconvolution, and TR with spectral whitening) but it can be more sensitive to noise.

The BG methodology can find application in key areas of geophysics. The resolution of RTM imaging can be enhanced by optimizing the focusing kernel of RTM. Another important application is improving the precision of earthquake or microseismic event location. Although the basic concepts of BG focusing are presented in this paper, certain modifications might be required on a case-by-case basis to customize the method for different applications.

7 ACKNOWLEDGEMENTS

We thank Simon Luo for the wave propagation code used to produce the results in this paper, and Diane Witters and Ken Larner for instructions on revision and editing. The software used to produce the results in the paper was written in Java with the use of libraries in the Mines Java Toolkit. This research was supported by the sponsors of the Center for Wave Phenomena at the Colorado School of Mines.

REFERENCES

Aki, K., and P. Richards, 1980, Quantitative seismology theory and methods: Freeman and Company.

Aster, R., B. Borchers, and C. Thurber, 2012, Parameter estimation and inverse problems second edition: Academic Press.

Aubry, J. F., M. Tanter, J. Gerber, J. L. Thomas, and M. Fink, 2001, Optimal focusing by spatio-temporal inverse filter. ii. experiments. application to focusing through absorbing and reverberating media: The Journal of the Acoustical Society of America, **110**, 48–58.

Backus, G., and F. Gilbert, 1968, The resolving power of gross earth data: Geophysical Journal of the Royal Astronomical Society, **16**, 169–205.

Behura, J., K. Wapenaar, and R. Snieder, 2012, Newton-marchenko-rose imaging: Image reconstruction based on inverse scattering theory: Technical Report CWP-720, Center for Wave Phenomena, Colorado School of Mines.

Berkhout, A., 1997, Pushing the limits of seismic imaging, part i: Prestack migration in terms of double dynamic focusing: Geophysics, **62**, 937–954.

Blomgren, P., G. Papanicolaou, and H. Zhao, 2002, Super-resolution in time-reversal acoustics: The Journal of the Acoustical Society of America, **111**, 230–248.

Broggini, F., R. Snieder, and K. Wapenaar, 2012, Focusing the wavefield inside an unknown 1d medium: Beyond seismic interferometry: Geophysics, **77**, A25–A28.

Fink, M., 1997, Time-reversed acoustics: Physics Today, **50**, 30–34.

———, 2006, Time-reversal acoustics in complex environments: Geophysics, **71**, 151–164.

———, 2008, Time-reversal waves and super resolution: Journal of Physics:Conference Series, **124**, 1–29.

Fink, M., W. Kuperman, J. Montagner, and A. Tourin, 2002, Imaging of complex media with acoustic and seismic waves: Springer-Verlag.

Haddadin, O., and E. S. Ebbini, 1998, Ultrasonic focusing through inhomogeneous media by application of the inverse scattering problem: Journal of the Acoustical Society of America, **104**, 313–325.

Larmat, C., R. A. Guyer, and P. A. Johnson, 2010, Time-reversal methods in geophysics: Physics Today, **63**, 31–35.

Larmat, C., J. Montagner, M. Fink, and Y. Capdeville, 2006, Time-reversal imaging of seismic sources and application to the great sumatra earthquake: Geophysical Research Letters, **33**, L19312.

Lu, R., 2002, Time reversed acoustics and applications to earthquake location and salt dome flank imaging: PhD Thesis, Massachusetts Institute of Technology.

Lu, R., and M. E. Willis, 2008, Locating microseismic events with time reversed acoustics: A synthetic case study: SEG Technical Program Expanded Abstracts, 1342–1346.

McMechan, G. A., 1982, Determination of source parameters by wavefield extrapolation: Geophysical Journal of the Royal Astronomical Society, **71**, 613–628.

———, 1983, Migration by extrapolation of time-dependent boundary values: Geophysical Prospecting, **31**, 413–420.

Montaldo, G., M. Tanter, and M. Fink, 2003, Real time inverse filter focusing through iterative time reversal: The Journal of the Acoustical Society of America, **115**, 768–775.

Nemeth, T., C. Wu, and J. T. Schuster, 1999, Least-squares migration of incomplete reflection data: Geophysics, **64**, 208–221.

Parker, R., 1994, Geophysical inverse theory: Princeton University Press.

Parvulescu, A., 1961, Signal detection in a multipath medium by m.e.s.s. processing: The Journal of the Acoustical Society of America, **33**, 1674.

Rentsch, S., S. Buske, S. Luth, and A. Shapiro, 2007, Fast location of seismicity: A migration-type approach with application to hydraulic-fracturing data: Geophysics, **72**, S33–S40.

Robert, J., and M. Fink, 2008, Greens function estimation in speckle using the decomposition of the time reversal operator: Application to aberration correction in medical imaging: The Journal of the Acoustical Society of America, **123**, 866–877.

Schuster, J. T., 2002, Reverse-time migration = generalized diffraction stack migration: 72nd Annual International Meeting, SEG, Expanded Abstracts, 1280–1283.

Schuster, J. T., S. Hanafy, and Y. Huang, 2012, Theory and feasibility tests for a seismic scanning tunnelling macroscope: Geophysical Journal International, **190**, 1593–1606.

Shapiro, S. A., 2008, Microseismicity a tool for reservoir characterization: EAEG.

Snieder, R., 2004, A guided tour of mathematical methods for the physical sciences, 2nd ed.: Cambridge Univ. Press.

Tanter, C., J. L. Thomas, and M. Fink, 2000, Time reversal and inverse filter: Journal of the Acoustical Society of America, **108**, 223–234.

Tanter, M., J. F. Aubry, J. Gerber, J. Thomas, and M. Fink, 2001, Optimal focusing by spatio-temporal inverse filter. i. basic principles: The Journal of the Acoustical Society of America, **110**, 37–47.

Ulrich, T., B. Anderson, C. Le Bas, P.-Y. Payan, J. Douma, and R. Snieder, 2012, Improving time reversal focusing through deconvolution: 20 questions: Proc. of Meetings on Acoustics, **16**, 045015.

Vellekoop, I., A. Lagendijk, and A. Mosk, 2010, Exploiting disorder for perfect focusing: Nature Photonics, **4**, 320–322.

Xuan, R., and P. Sava, 2010, Probabilistic microearthquake location for reservoir monitoring: Geophysics, **75**, MA9–MA26.

APPENDIX A: OPTIMIZATION OF THE RTM FOCUSING KERNEL

We use the Backus and Gilbert method to optimize the RTM focusing kernel (see section 5.2) for each receiver in a shot gather for a specific target in the model space.

For weak scattering, the scattered data recorded at receiver location $\mathbf{r}_g$ with a source at $\mathbf{r}_s$ can be written in the frequency domain in terms of the Born approximation to the Lippmann-Schwinger equation (Schuster, 2002):

$$d(\mathbf{r}_g, \mathbf{r}_s) = \int G(\mathbf{r}_g, \mathbf{r})\, W\, G(\mathbf{r}, \mathbf{r}_s)\, \mathbf{m}(\mathbf{r})\, d\mathbf{r}, \qquad \text{(A1)}$$

where $G(\mathbf{r}_g, \mathbf{r})$ is the Green's function for the Helmholtz equation for a specified background medium with a source at $\mathbf{r}$ and receiver at $\mathbf{r}_g$, $G(\mathbf{r}, \mathbf{r}_s)$ is the Green's function for the same medium with a source at $\mathbf{r}_s$ and receiver at $\mathbf{r}$, $\mathbf{m}(\mathbf{r})$ represents the reflectivity distribution perturbed from the background, and W represents the source wavelet function. The integration is over the model space.

Using RTM equation 12 written in the frequency domain for N geophones at locations $\mathbf{r}_{g_i}$ where $i = 1, 2, ..., N$, the reflectivity value at a target location $\mathbf{r}_f$ can be expressed as a weighted sum of data

$$\mathbf{m}_{mig}(\mathbf{r}_f) = \sum_{i=1}^{N} a_i\, d(\mathbf{r}_{g_i}, \mathbf{r}_s), \qquad \text{(A2)}$$

where the complex weights a_i are

$$a_i = G^*(\mathbf{r}_{g_i}, \mathbf{r}_f)\, W^*\, G^*(\mathbf{r}_f, \mathbf{r}_s), \quad i = 1, 2, ..., N. \qquad \text{(A3)}$$

Note that a_i in A3 is the complex conjugate of the RTM focusing kernel defined in equation 13.

Inserting $d(\mathbf{r}_g, \mathbf{r}_s)$ from A1 into A2 and changing the order of integration and summation gives

$$\mathbf{m}_{mig}(\mathbf{r}_f) = \int [\sum_{i=1}^{N} a_i\, G(\mathbf{r}_{g_i}, \mathbf{r})\, W\, G(\mathbf{r}, \mathbf{r}_s)]\, \mathbf{m}(\mathbf{r})\, d\mathbf{r}. \qquad \text{(A4)}$$

The bracketed factor in A4 is an averaging kernel that we would ideally like to closely approximate a Dirac delta function with spatial support at $\mathbf{r}_f$, i.e.,

$$\sum_{i=1}^{N} a_i\, G(\mathbf{r}_{g_i}, \mathbf{r})\, W\, G(\mathbf{r}, \mathbf{r}_s) \to \delta(\mathbf{r} - \mathbf{r}_f). \qquad \text{(A5)}$$

Our goal here is to determine new coefficients a_i' (instead of a_i defined in A3) such that the deltaness criterion A5 is satisfied as closely as possible. This goal can be achieved, for example, by minimizing an objective function of the form

$$J = \int |\sum_{i=1}^{N} a_i'\, G(\mathbf{r}_{g_i}, \mathbf{r})\, W\, G(\mathbf{r}, \mathbf{r}_s) - \delta(\mathbf{r} - \mathbf{r}_f)|^2 d\mathbf{r}, \qquad \text{(A6)}$$

where the integration is carried out over the model space.

Minimizing A6 gives a linear system of the form

$$\Gamma \mathbf{a}' = \mathbf{a}, \qquad \text{(A7)}$$

where Γ is an $N \times N$ matrix with elements

$$\Gamma_{ij} = \int G(\mathbf{r}_{g_i}, \mathbf{r})\, G^*(\mathbf{r}_{g_j}, \mathbf{r})\, G(\mathbf{r}, \mathbf{r}_s)\, G^*(\mathbf{r}, \mathbf{r}_s)\, d\mathbf{r}, \quad i, j = 1, 2..., N, \qquad \text{(A8)}$$

and $\mathbf{a}$ is an $N \times 1$ vector with elements defined in A3.

Solving equation A7 gives the $N \times 1$ vector $\mathbf{a}'$ of optimized kernels that can be used as enhanced migration focusing kernels in generalized diffraction-stack migration.